MODELLING OF MULTI-COMPONENT FUEL DROPLETS HEATING AND EVAPORATION

MODELLING OF MULTI-COMPONENT FUEL DROPLETS HEATING AND EVAPORATION

AHMED ELSAID YN6SYD.654667(L)1.63p701( )-0F16W
requirements f he niversity f righton
for the degree of octor of hilosophy

January 2012

Contents

Abstract i

Contents ii

List of figures vi

List of tables xv

Acknowledgements xvi

Declaration xvii

Nomenclature xviii

1 General introduction 1

1.1 Background 1
1.2 Objectives 3
1.3 Layout of the thesis 4
1.4 Dissemination of the results 4

2 Literature review 5

2.1 Mono-component droplet heating and evaporation 5
2.2 Multi-component modelling 14
  2.2.1 Discrete component models 14
  2.2.2 Many components models 17
2.3 Experimental studies 22
2.4 Conclusions of Chapter 2 27

3 Monodisperse mono-component fuel droplets heating and evaporation 30

3.1 Introduction 30
Model 31
  3.2.1 Droplet heating 31
  3.2.2 Droplet evaporation 32
3.3 Experimental set-up 33
3.4 Results 37
3.5 Conclusions of Chapter 3 46

4 A simplified model for bi-component droplet heating and evaporation 48

4.1 Introduction 48
4.2 Basic equations and approximations 49
    4.2.1 Droplet heating 49
    4.2.2 Droplet evaporation 49
    4.2.3 Species diffusion in the liquid phase 50
    4.2.4 Species mass fractions at the surface of the droplet 52
    4.2.5 Moving boundary effects 53
    4.2.6 Numerical solutions 55
4.3 Experimental data and input parameters 55
4.4 Results 57
    4.4.1 Solution A based on stationary boundary 57
    4.4.2 Solutions A and B (stationary boundary) 65
    4.4.3 Solution A based on moving boundary 73
    4.4.4 Effects of the binary diffusion coefficient 78
4.5 Conclusions of Chapter 4 84

5 Coupled solution and code optimisation 86

5.1 Introduction 86
5.2 Basic equations and approximations 86
5.3 The coupled solution 88
    5.3.1 Mass balance 89
    5.3.2 Heat balance 90
    5.3.3 Size of the region of influence 91
5.4 Numerical algorithm 91
5.5 Input parameters 93
5.6 Results 94
5.7 Accuracy versus CPU efficiency 105
5.8 Conclusions of Chapter 5 112

6 A quasi-discrete model for heating and evaporation of complex multi-component hydrocarbons fuel droplets 114

6.1 Introduction 114
6.2 Quasi-discrete model 115

6.3 Thermo-physical properties 117
6.3.1 Saturated vapour pressure 117
6.3.2 Latent heat of evaporation 117
6.3.3 Critical and boiling temperatures 118

List of figures

Fig. 2.1 Definition of the probe volume, Lavieille et al (2002b). 24
Fig. 2.2 Experimental set-up used by Castanet et al (2002). 25
Fig. 2.3 Classifications of fuel droplet heating and evaporation models according to fuel composition (a) and droplet’s boundary state (b). 27
Fig. 2.4 Summary of heating and evaporating models for mono-component droplets (a) and multi-component droplets (b). 28

Fig. 3.1 Layout of the heated enclosure and the droplet generator used by Deprédurand et al (2010). 34
Fig. 3.2 The plots of the time evolution of the experimentally observed temperatures of acetone droplets for Case 1, and temperatures at the surface of these droplets (T_s), average temperatures in the droplets (T_{av}) and the temperatures at the centre of the droplets (T_c)

heptane, n-decane and n-dodecane droplets for Case 2 are shown. The input parameters of the models were taken from Table 3.1. 43
Fig. 3.11 The same as Fig. 3.10 but for $_d/_{d0}$ 44
Fig. 3.12 The same as Fig. 3.10 but for Case 3, except without the results for 3-pentanone. 45
Fig. 3.13 The same as Fig. 3.12 but for $_d/_{d0}$ 45

Fig. 4.1 Experimentally observed velocities for pure acetone droplets (triangles) approximated by Eq. (3.7). 56
Fig. 4.2 The time evolution of droplet surface, average and centre temperatures (T_s, T_{av}, and T_c) and experimentally observed temperatures for pure acetone droplets with initial diameter 143.4 µm and homogeneous temperature 34.8 °C in an ambient gas at temperature equal to 21.5 °C. 58
Fig. 4.3 The same as Fig. 4.2 but for pure ethanol droplets with initial diameter 140.8 µm, homogeneous temperature 38.0 °C and ambient gas temperature equal to 22.0 °C. 58
Fig. 4.4 The same as Figs. 4.2 and 4.3 but for the 25% ethanol–75% acetone mixture droplets with initial diameter 133.8 µm, homogeneous temperature 32.8 °C and ambient gas temperature equal to 21.1 °C. The results of calculations based on the ideal (**1**) and non-ideal models are presented. 60
Fig. 4.5 The same as Fig. 4.4 but for the 50% ethanol–50% acetone mixture droplets with initial diameter 142.7 µm, homogeneous temperature 37.5 °C and ambient gas temperature equal to 20.8 °C. 60
Fig. 4.6 The same as Figs. 4.4 and 4.5 but for the 75% ethanol–25% acetone mixture droplets with initial diameter 137.1 µm, homogeneous temperatures 38.6 °C and ambient gas temperature equal to 21.6 °C. 61
Fig. 4.7 The same as Fig. 4.6 but including additional results of calculations of T_s and T_{av} (based on the vortex model, as reported in Maqua et al. 2008b) instead of the results referring to T_c. 62
Fig. 4.8 The plots of $_d$ versus time predicted by the ideal (**1**) and non-ideal,

Fig. 4.10 The plots of the ethanol mass fraction Y_e versus $/ \;_d$ for six moments of time after the start of calculations for the same droplets as in Figs. 4.6-4.9. 64

Fig. 4.21 The same as Fig. 4.20 but for the mass fractio

Fig. 5.7 The plots of d

the solution to the temperature equation equal to 100 for the same conditions as in Fig. 5.2. Calculations were performed on 3 GHz CPU, 3 GB RAM work station. . 108

Fig. 5.18 The plots of relative errors (in percent) of calculation of droplet surface, average and central temperatures (T_s, T_{av} and T_c) and CPU time versus the number of terms in the solutions to the temperature and species equations (these numbers are assumed equal) for the same conditions as in Fig. 5.2. Calculations were performed on 3 GHz CPU, 3 GB RAM work station. 109

Fig. 5.19 The plots of relative errors (in percent) of calculation of liquid n-decane mass fractions at the surface of the droplet, average mass fraction and the mass fraction at the centre of the droplet (Y_s, Y_{av} and Y_c) and CPU time versus the number of terms in the solutions to the temperature and species equations (these numbers are assumed equal) for the same conditions as in Fig. 5.2. Calculations were performed on 3 GHz CPU, 3 GB RAM work station. 109

Fig. 5.20 The plots of the predicted droplet surface temperatures versus for different timesteps for the 95% n-decane – 5% 3-pentanone mixture (Case 1) at 5 ms after the start of calculations. 111

Fig. 5.21 The plots of average temperatures T_{av} with different values indicated at the curve versus time for the same conditions as in Fig. 5.2. 112

Fig. 6.1 The plots of versus n as predicted by Eq. (6.15). 118

Fig. 6.2 The plots of and , and their Approximations (6.16) and (6.17), versus n

experimental values of for = 300 K in the range **5** **18**, inferred from NIST website (filled squares) and van Miltenburg (

Fig. F

List of tables

Table 3.1 The values of , , d, $\%_{\&'}$, $\%_{()}$, $_*$ and $_+$ for three experiments with acetone, ethanol, 3-pentanone, n-heptane, n-decane and n-dodecane droplets (abbreviated as acet, ethan, 3-pen, n-hep, n-dec n-dod). In the case of n-decane and n-dodecane, the values of

Declaration

I declare that the research contained in this thesis, unless otherwise formally indicated within the text, is the original work of the author. The thesis has not been previously submitted to this or any other university for a degree, and does not incorporate any material already submitted for a degree.

Signed

Date

Nomenclature

English Symbols

	Constant introduced in Eq. (2.4) or parameter introduced in Eqs. (6.16) and (6.17)
A	Parameter introduced in Eq. (6.12)
A	Parameters defined by Eqs. (6.24)
A_{ρ} ρ ρ	Parameters defined by Eqs. (6.19)
	Constant introduced in Eq. (2.4), parameter introduced in Eqs. (6.16) and (6.17) or parameter defined by Eq. (6.21)
	Parameter introduced in Eq. (6.12) (6.17) Eqs. E6.16 n

2	Limiting values of
	Thermal conductivity [W/(m.K)]
	Boltzmann constant [J/K]
	Parameter defined at Eq. (5.16)
	Parameter introduced at Eq. (2.23)
	Steady-state evaporation constant [m^2/s]
L	Latent heat of evaporation [J/kg]
L_d	Diffusion length [m]
Le	Lewis number
	Molecular weight [kg/kmole]
B_D	Instantaneous droplet vaporization rate [kg/s]
n	Parameter introduced in Eq. (2.8) or number of carbon atoms
	Number of moles or number of terms
Nu	Nusselt number
p	Pressure [Pa]
Pe	Peclet number
Pr	Prandtl number
	Power spent on the droplet heating [J/s]
q_n	Parameter introduced in Eq. (2.23) or defined by Eq. (4.20)
$*$	Normalized radius introduced in Eq. (2.38)
	Distance from the centre of a spherical droplet [m]
E_D	Rate of change of radius [m/s]
E_{DF}	Rate of change of radius due to evaporation [m/s]
E_D	Rate of change of radius due to thermal expansion/contraction [m/s]
Re	Reynolds number
u	Universal gas constant [8.314472 J/(K.mole)]
Sc	Schmidt number
Sh	Sherwood number
	Time
	Temperature
	Time at the beginning of timestep [s]
	Time at the end of timestep [s]
	Characteristic duration of the process [s]

G^{H}	Dimensionless time defined by Eq. (5.1)
u	Velocity [m/s]
$*$	Constant introduced at Eq. (3.7) [m/s]
$+$	Constant introduced at Eq. (3.7) [m/(s.ms)]
	Volume [m^3]
V	Radial velocity of the vapour defined by Eq. (5.2) [m/s]
X	Mole fraction
Y	Mass fraction

Greek symbols

I	Parameter of the distribution function or parameter defined by Eq. (4.6)
I_7	Parameter defined by Eq. (4.14)
J	Parameter of the distribution function
	Activity coefficient defined by Eq. (E.3) or parameter of the distribution function
G	Timestep
$K_{,M}$	Thermal and mass film thicknesses defined by Eqs. (5.3) and (5.4) [m]
N	Evaporation rate of any of the species defined by Eq. (4.7)
%	$\frac{Sh}{Sh_{0RS}}$ $\frac{Nu}{Nu_{0RS}}$
V	Dimensionless temperature introduced by Eq. (2.20)
W	Thermal diffusivity [m^2/s]
$X_{Y,Z}$	Eigenvalues
	Dynamic viscosity [Pa.s]
$_{Y}$ G	Parameter introduced in Eq. (2.23)
[	Kinematic viscosity [m^2/s]
$\backslash]_{Z} \backslash^{+}$	Parameter introduced in Eq. (2.23), defined by Eq. (4.19) or defined by Eq.(4.24)
^	Parameter introduced in Eq. (2.18)
ρ	Density [kg/m^3]

/	Minimal distance between molecules [Angstrom]
_	Parameter defined by Eq. (2.33)
	Parameter introduced in Eq. (2.13) and Eq. (4.8)
`	Parameter introduced in Eq. (2.18)

Subscripts

a	Air
atm	Atmospheric
av	Average
	Boiling
c	Droplet centre
c	Critical
d	Droplet
eff	Effective
	Fuel
[illegible]	Gas or region of influence
u	Heat-up
iso	Isolated droplet
	Liquid
e	Reference
	Droplet surface
	Steady-state
	Temperature
[illegible]	Vapour
Y	Species diffusion
0	Initial or beginning of timestep
1	End of timestep
∞	Far from the droplet surface

1 General introduction

1.1 Background

1.2 Objectives

The objectives of this thesis are the following:

1. To perform a comparison between the predictions of the heating and evaporation model, suggested by Sazhin et al (2004), and experimental data similar to those reported by Deprédurand et al (2010) for mono-component droplets, but for a wider range of substances (acetone, ethanol, 3-pentanone, n-heptane, n-decane and n-dodecane) and different experimental conditions. The effect of interaction between droplets on the predicted droplet temperatures and radii will be taken into account.

2. To develop a simplified model for multi-component droplets (small number of components) based on a new analytical solution to the species diffusion equation inside the droplet and validation of this model using the available experimental data (aceton

6. To develop a new quasi-discrete model for multi-component fuel droplets with large number of components and to apply this model to Diesel and gasoline fuels.

1.3

2 Literature review

This chapter briefly highlights numerous previous studies related to heating and evaporation of fuel droplets. Section 2.1 focuses on the models of mono-component droplets heating and evaporation. Section 2.2 focuses on the models of multi-component droplets heating and evaporation. Experimental studies related to the heating and evaporation process of fuel droplets are summarised in Section 2.3. A summary of this chapter is presented in Section 2.4

2.1 Mono-component droplet heating and evaporation

Chin and Lefebvre (1983a) studied the effect of ambient pressure and temperature on the evaporation rate of different types of fuels (aviation gasoline, n-heptane, JP4, JP5 and DF2) in air. They provided the following equation to calculate the steady-state evaporation constant $b_?$ (see Eq. (2.7)) of the d^2-law:

$$b_? \quad \frac{c_d\, e f\, *g 2_h}{9\, i_d}, \qquad (2.1)$$

where j_k is the gas specific heat capacity, χ is the gas thermal conductivity, is the liquid fuel density and $_M$ is the Spalding mass transfer number:

$$_M \quad \frac{l_{mn}\, o\, l_{mp}}{*\, o\, l_{mn}} \quad q\frac{l_{mn}}{*\, o\, l_{mn}} r_{l_{mp}\, sY}, \qquad (2.2)$$

where t_u and t_{uv} are the fuel vapour mass fraction at the droplet surface and in the surroundings respectively. They assumed that t_{uv} **0**, while t_u was calculated from the following equation:

$$t_u \quad x\mathbf{1} < 5\frac{j}{j_m} \; ; \; \mathbf{1} : \frac{M_y}{M_z}\{^{o*}, \qquad (2.3)$$

where $|$ is the ambient pressure, $\}_{,\sim}$ is the molecular weight of air, $\}_{\#}$ is the molecular weight of fuel and $|_u$ is the fuel vapour pressure (saturation pressure) at the droplet surface calculated from the Clausius-Clapeyron equation:

$$|_u \quad \mathbf{exp} \quad ; \quad / \quad ; \mathbf{43}, \qquad (2.4)$$

where is the droplet surface temperature and , are constants specified for various types of fuel.

They suggested a numerical procedure ons ts numpresen fi2 available for heating the droplet is equal to the heat used in evaporation of the droplet which means that$_{,?}$ $\mathbf{const}$

was also noticed that increasing ambient temperature reduced both heat-up and steady-state periods.

Abramzon and Sirignano (1989) developed a model for mono-component droplets heating and evaporation. This model considered the effects of variable thermophysical properties, the non-unity Lewis number in the gas film, internal recirculation inside the droplet and the transient heating of liquid fuel droplets. They called this model the 'extended model'. It is based on the solution of a two dimensional (axially symmetric) energy equation inside the droplet. The limiting cases of this model are: for small liquid Peclet numbers $Pe_{d(l)}$ the extended model is reduced to the 'Conduction limit model' while for high liquid Peclet numbers the extended model represents the 'Vortex model'.

It was noticed that the extended model has poor CPU efficiency and is not adequate for implementation into CFD codes. A simplified model was suggested to take into account the effect of recirculation inside droplets via the ETC model, in which the thermal conductivity of liquid is multiplied by the factor which allows for the effect of internal circulation on heat transfer within the droplet:

$$ii \quad , \qquad (2.13)$$

where the coefficient varies from 1 (at droplet Peclet number $Pe_{d(l)} = Re_{d(l)} Pr_{d(l)} <$ 10) to 2.72 (at $Pe_{d(l)} > 500$) and it was approximated as:

$$\mathbf{1.86 < 0.86tanh¤2.225log_{*Y}¦Pe_D \ /30¨©}, \qquad (2.14)$$

where $\mathbf{Re}_D \quad \frac{+ \ _9 ' n 7_8}{«_9}$ is the Reynolds number and $\mathbf{Pr}_D \quad \frac{_9«_9}{_9}$ is the Prandtl number, based on liquid transport coefficients, ρ, , and are liquid density, dynamic viscosity, specific heat capacity and thermal conductivity respectively and is the maximum surface velocity calculated as:

$$\frac{*}{+} - \ _k \ ; \quad _D - 5\frac{«_d}{«_9} : \mathbf{Re}_D \ ®, \qquad (2.15)$$

where $_k$ is the gas velocity, $_D$ is the droplet velocity, $_k$ is the gas dynamic viscosity, $\mathbf{Re}_D$ is the Reynolds number based on gas transport coefficients $\mathbf{Re}_D$ $\mathbf{2} \ _k - \ _k \ ; \ _D - E_D \overline{\ } \ _k$ and $_®$ is the friction drag coefficient:

$$® \quad \frac{*+. \ °}{7±_8^{2/3} \ *g2_h}, \qquad (2.16)$$

where $_M$ is the Spalding mass transfer number defined by Eq. (2.2).

The predictions of the ETC and extended models almost coincided while the extended model results appeared to be in between the results of the

Conduction limit models. The ETC model does not detail the physical features of the recirculation inside the droplet which are not important in most practical engineering applications but it predicts the global effect of the recirculation on heat transfer inside the droplet. To improve the accuracy of this model, a dimensionless temperature V ; Y †¦ k ; Y¨ was introduced. The dimensionless surface temperature was calculated as:

V ¸ ¹⁰ gY•+» / ¼ , ; •€• ;^34

$$\mathrm{OP} \qquad \frac{\mathrm{ef}\ {*}\mathrm{g2}\quad {}_{\mathrm{h}}}{2_{\mathrm{h}}}\ \text{¤}\ < \mathrm{w}\bullet\$^{\mathrm{a}}\bullet\ {}^{*}_{\mathrm{D}}\ {}^{+}$$

The model referred to as ‘M3’ is a limiting case of ‘M4’ when 3 M 3 . When the coefficient 0.3 in Eqs. (2.28) and (2.29) was replaced by 0.276 the model was referred to as ‘M5’. The ‘M6’ model was based on the analysis of the experimental data:

OP + 2 h X *gY•œ™áÓ Ô† ² 8 (Õ Ô† ³ 8 / *g2 h Æ•Û { , (2.36)

TU ef *g2 ‚ / 2‚ X +gY•áØÓ Ô† ² 8 Ö× Ô† ³ 8 / *g2 â Æ•Û { , (2.37)

where ® Ï im ¦ d o n ¨ / • 5 ; • Ò / • ã : and ‘ is the heat transferred to the droplet by convection.

Sazhin et al (2006) pointed out that the ‘M4’ model predicts the evaporation time closest to the one obtained based on the approximation of experimental data. They showed that the ETC model leads to marginally better agreement with experimental data than the ITC model. This is in agreement with the results of Bertoli and Migliaccio (1999).

Barata (2008) presented a numerical study for evaporation of biofuel droplets injected through a turbulent cross-stream. The effect of interaction between droplets was ignored and the ITC model was used to describe the heating process inside the liquid droplet. This model was applied to the analysis of the evaporation of Diesel ‘DF2’, Rapeseed Methyl Ester ‘RME’, ethanol and n-heptane fuel droplets. The results showed that ‘RME’ has similar evaporation c

Mitchell et al (2011) suggested a numerical solution to the heat conduction equation inside the droplet considering the effect of changes in radius during the individual timesteps. The predictions of their model coincided with those of the model based on the analytical solution to this equation provided by Sazhin et al (2010a).

Sazhin et al (2011d) suggested other analytical solutions to the heat conduction equation inside the droplet considering the effect of changes in radius during the individual timesteps, assuming that the time evolution of the droplet radius is known. The predictions of these calculations were compared with the predictions obtained using their previously suggested approach when the droplet radius was assumed to be a linear function of time during individual timesteps (Sazhin et al, 2010a). For sufficiently small timesteps the time evolutions of droplet temperatures and radii predicted by both methods coincided. The solutions suggested by Sazhin et al (2010a, 2011d), predict lower droplet temperature and slower evaporation when the effects of the reduction of R_d are taken into account.

2.2 Multi-component modelling

When modelling multi-component fuel droplets one needs to take into account that different components evaporate at different rates and this leads to concentration gradients and d the mass balance was used to calculate the evaporation rate of the multi-component droplets. The model was then implemented into KIVA3 CFD code and applied to evaporation of isolated droplets, Diesel spray and Diesel engine conditions. Different simulate the heating of the liquid phase. The acous

where ê is the property of the component (they used the molecular weight to represent this property), ê is the origin, I and J are parameters that determine the shape of the distribution and determines the original shift. They built their analysis of the liquid phase on the 'ID' and 'ITC' models. For the liquid-vapour equilibrium they used Raoult's law with the Clausius-Clapeyron. The model was applied to the analysis of evaporation of Diesel and gasoline fuels.

Lippert and Reitz (1997) applied the continuous thermodynamics approach to multidimensional calculations for droplets and sprays. Similarly to Tamim and Hallett (1995), the Gamma distribution (Eq. (2.40)) was used, the droplets were assumed to have uniform temperature and a well mixed liquid phase (ITC and ID continuous thermodynamics approach. This model was shown to be independent of the form of the distribution function that is selected for the continuous fuel species and they used the Gamma distribution. They derived the transport equations for the semi-continuous systems. The liquid phase included liquid fuel (continuous) and the ambient gas (discrete) while the gas phase included fuel vapour (continuous) and the ambient gas (discrete). The model was applied to modelling of evaporation of Diesel fuel with composition parameters similar to those used by Tamim and Hallett (1995) and evaporation of n-tridecane as mono-component fuel with I ww•w , J w• and ñ •w and with the mean molecular weight corresponding to Diesel fuel. The droplets were injected into nitrogen and the results showed that for high pressure conditions the heat of vaporization increases to a maximum value then decreases with increasing temperature. For low pressures the heat of vaporization decreased with increasing temperature. The equivalent mono-component fuel (n-tridecane) predicted smaller heat of vaporization especially at low droplet temperatures and high ambient pressures conditions. They emphasised the importance of considering the composition of multi-component fuels under sub- and super-critical pressure conditions.

Arias-Zugasti and Rosner (2003) introduced spectral representation of the PDF with a number of components (pseudo-components) much smaller than the number of components in the original chemical mixture. They generalised the former method in which the PDF describing the mixture was assumed continuous thermodynamics technique. They considered two cases of the distribution function. The first was the single distribution function and the second was a sum of two distribution functions with widely differing molecular weights (n-heptane and n-dodecane, a ‘dumbbell mixture’). The results using the single distribution function showed that neither temperature nor evaporation rate are significantly affected by internal mixing until near the end of the droplet's lifetime. The results indicated that the largest effects of the liquid mixing models are seen for two discrete components and these effects decrease when the discrete components are replaced by two broad distributions to form a dumbbell mixture.

the effect of finite thermal diffusivity but assumed infinite mass diffusivity for the liquid phase. The results showed good agreement with the experimental data.

Zhang and Kong (2010) developed a hybrid vaporization model based on both the continuous thermodynamics approach, to describe petroleum fuels, and the discrete components approach, to represent biofuels and mono-component substances. It was assumed that liquid phase heat and mass diffusivities were represents the bulk of the fuel, a small light FAME fraction reproduces the early part

1997), which is based on the variation of the refractive index of the droplet with temperature. A visible laser beam passes through the droplet and produces a rainbow pattern. The rainbow pattern location, which changes with temperature, determines fluorescence ratio. This ratio was found to be independent of laser power within 1%, corresponding to an error in the temperature of less than 0.5 ºC, and it does not change with the change of the measuring volume size. Lavieille et al (2002a) demonstrated the ability of the two-colour LIF technique to provide average within the injector body. For specific frequencies of forced mechanical vibration, the liquid jet broke up into equally spaced and mono-sized droplets.

Castanet et al (2002) implemented electrostatic deviator plates at the injector exit in order to adjust the droplets spacing without changing the droplet diameter. The droplets stream then passed through the thermal boundary layer of a heated vertical plate as shown in Fig. 2.2. The droplet size was measured using a light scattering technique (interferential method) while the droplet velocity was measured by Laser Doppler Velocimetry (LDV). Measured droplet temperature, velocity and size were used to estimate the heat fluxes acting on the evaporating droplets for both heat-up process and steady-state of evaporation. The results showed that the heat convection coefficient for the heat-up process is higher than the one in the steady evaporation case. It was also demonstrated that corrections to the Nusselt number have to be applied to compensate for the effect of interaction between droplets.

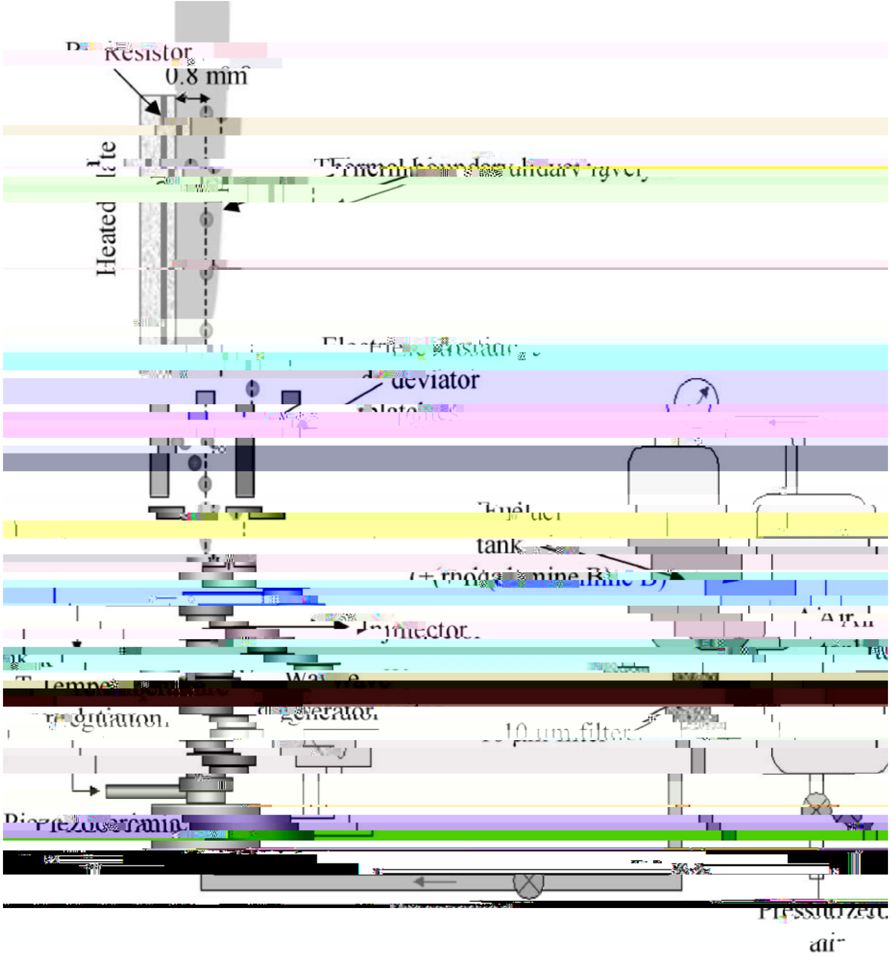

Fig. 2.2 Experimental set-up used by Castanet et al (2002).

Castanet et al (2005) used phase Doppler anemometry for measurement of droplet sizes and calculated the heat fluxes (radiant flux, evaporation flux and convective heat flux) acting on evaporating ethanol droplets moving into a flame. The Nusselt and Sherwood numbers were calculated from the heat fluxes and corrections to them were presented to take into account the effect of interaction between droplets in the following form: %

% $\frac{,^{-}}{,^{-}\ \text{òóô}}$ $\frac{()}{()\ \text{òóô}}$ Œ£ŠPw•$¢ ; w• L (2.41)

where is the distance parameter, defined as the droplet spacing divided by their diameter. The subscript iso refers to isolated droplets. For distance parameter larger than 9, the interaction effects were shown to be negligible. For distance parameters less than 9, the evaporation rate was shown to decrease with increasing values of the distance parameter.

Maqua et al (2008a) extended the experiments described by Castanet et al (2005) to evaporation of ethanol and acetone as mono-component droplets. The measure droplets. A brief description of these experiments will be presented where they provide validation of our models.

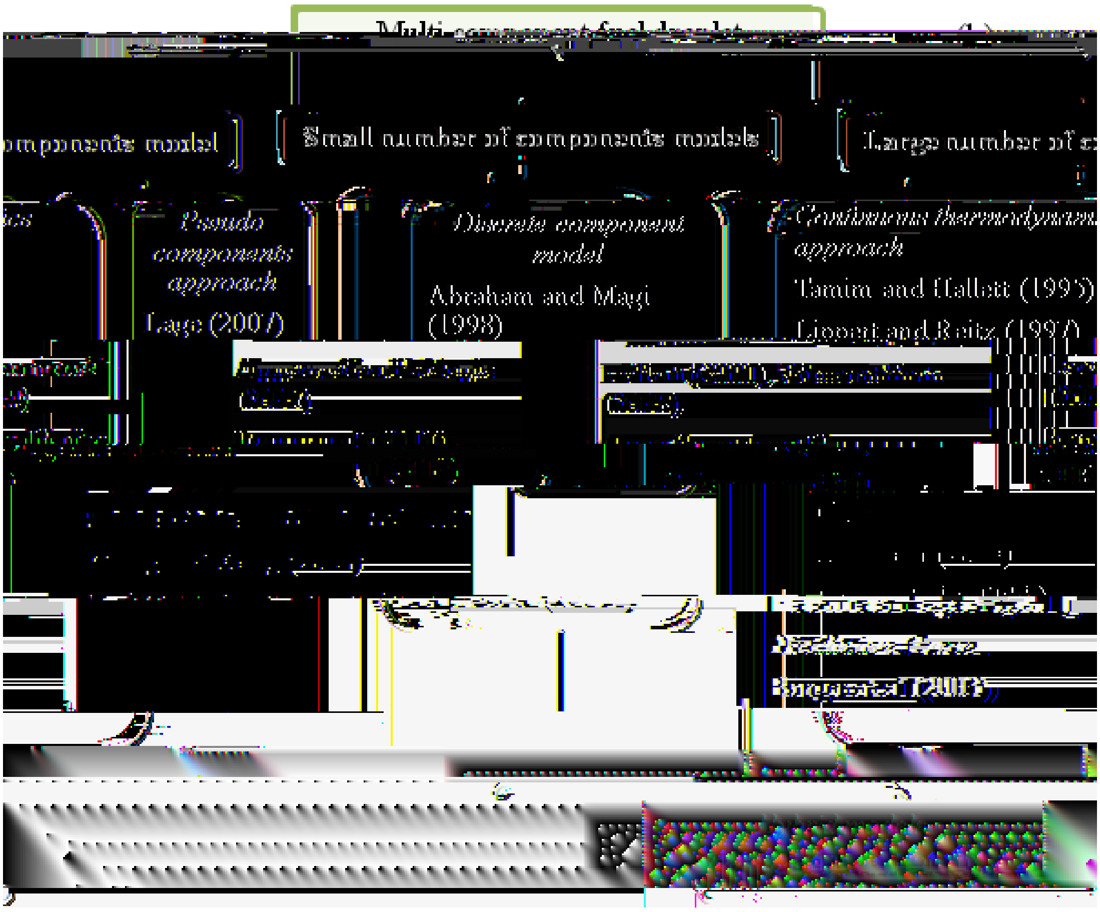

Fig. 2.4 Summary of heating and evaporating models for mono-component droplets (a) and multi-component droplets (b).

3 Monodisperse mono-component fuel droplets heating and evaporation

3.1

The value of Sh_{iso} for an isolated moving droplet is estimated based on the so-called ‘M4’ model via Eq. (2.30) (Abramzon and Sirignano, 1989; Sazhin et al 2006).

The values of the transport coefficients were taken for air at the reference temperature ±# k <¦ k ; ¨†$ (Incropera and DeWitt, 2002; Sazhin, 2006). The contribution of fuel vapour to the transport properties of air and the effects of droplets on air are ignored at this stage.

3.3 Experimental set-up

Droplet diameters and average temperatures were measured using the experimental set-up at the University of Nancy (France), which is described in a number of papers and theses, including (Deprédurand, 2009; Deprédurand et al, 2010). This will be only briefly summarised below.

Linear monodisperse droplet streams were generated by Rayleigh disintegration of a liquid jet undergoing vibration generated in a piezoelectric ceramic. The fuel was pre-heated in the injector by means of externally heated circulating water. The temperature of the fuel was measured exactly at the injection point with a K type thermocouple situated within the injector body. For specific frequencies of forced mechanical vibration, the liquid jet broke up into equally spaced and mono-sized droplets. The droplets were then injected into an enclosure fed with hot air coming from an electrical heater. In order to limit the thermal losses, a resistive electrical wire was inserted within the enclosure wall so that the wall temperature could be regulated to match that liquid fuel with a small quantity of a fluorescent tracer, pyromethene 597- C8. An interesting feature of pyrromethene 597-C8 relates to its temperature sensitivity that is almost unchanged when dissolved into any of the selected fuels (Deprédurand et al, 2008). The ratio of the fluorescence intensity detected in two spectral bands is a function of the temperature regardless of laser intensity, time-dependent tracer concentration, and measurement volume (Deprédurand et al, 2008). The velocity of the droplets was measured by Laser Doppler Velocimetry using the same laser light source as for the fluorescence excitation. The droplet size reduction was determined using the light scattering in the forward direction, where a stationary interference pattern is created.

Six liquid fuels were tested: acetone, ethanol, 3-pentanone, n-heptane, n-temperatures and radii, starting from the moment when the first droplet was observed near the entrance to the enclosure. By placing a thermocouple at different locations it was established that air temperature $_k$ did not vary inside the chamber. Hence, it was considered to be constant during each experiment in the modelling. The droplet absolute velocities were approximated as linear functions of time (measured from the moment of injection):

$$_D \quad _* \; ; \quad _+ G, \tag{3.7}$$

where constants $_*$ and $_+$ were determined for each experiment (Table 3.1), alongside the ratios $\%_{;L}$ $.TU \dagger TU_{QRS}$ and $\%_{()}$ $OP \dagger OP_{QRS}$, describing the effects of interaction between droplets in the stream, where subscript $_{iso}$ refers to isolated droplets. The error of determination of $_D$ is comparable with the ambient air velocities up to 0.3 m/s. This justifies the assumption that the absolute droplet velocities, estimated by Eq. (3.7), are equal to droplet velocities relative to ambient air. These velocities were used for the estimation of the Nusselt and Sherwood numbers for isolated droplets, Deprédurand et al. (2010).

The values of the Nusselt and Sherwood numbers were estimated based on simultaneous measurements of droplet sizes and mean temperatures. These measurements allowed the evaluation of heat fluxes responsible for droplet heating and evaporation rates. These rates, alongside the measured time evolution of droplet mean temperatures, were used for the estimate of the convective heat flux, responsible for droplet heating, and mass flux of fuel vapour leaving the droplet. The main difficulty in converting these estimates into the estimates of the Nusselt and Sherwood numbers relates to the fact that the surface droplet temperatures were not directly measured and had to be estimated. This issue is addressed in (Deprédurand, 2009; Deprédurand et al, 2010), where

ŽDY (measured directly when the first droplets near the entrance to the enclosure were observed), %, , %() , * and + for each experiment are presented in Table 3.1, alongside boiling and critical temperatures (and) for each substance (Poling et al, 2000). The values of C are shown to indicate the closeness of droplets in these experiments.

Case	Parameter	Acet	Ethan	3-Pen	n-Hep	n-Dec	n-Dod
	T						

s heating and evaporation

T_{av}, studied for Case 1, the analysis for Cases 2 and 3 is focused on the difference between these temperatures and the initial droplet temperatures T_0. The corresponding plots for T_{av} - T_0 versus time for Case 2 for all six substances are shown in Fig. 3.10. As follows from this figure, although the trends predicted by the model are similar to the ones observed experimentally, there are noticeable deviations between the actual values of predicted and observed average droplet temperatures. The maximal deviation between them is seen for n-decane and n-dodecane droplets. The minimal deviation between them is seen for 3-pentanone droplets.

Fig. 3.12 The same as Fig. 3.10 but for Case 3, except without the results for 3-pentanone.

observed ones by up to about 8 °C, and the actual values of the predicted droplet radii can differ from the observed ones by up to about 12%. Combining the above results and those reported previously by Maqua et al. (2008a), it could be concluded that the ETC model, based on the analytical solution to the heat conduction equation inside droplets, can predict the observed average temperature of droplets with possible errors not exceeding several °C, and observed droplet radii with possible

models) for measurements of droplet temperatures in monodisperse bi-component (ethanol/acetone) droplet streams is briefly described in Section 4.3. In Section 4.4, some results of the numerical solutions to the basic equations for the values of parameters relevant to the experimental set-up described in Section 4.3 are presented. In Section 4.5 the results, based on analytical and numerical solutions to the equations of heat transfer and species diffusion inside droplets, are compared for experimental conditions described in Section 4.3. In Section 4.6 the results, taking and not taking into account the effects of moving boundary, predicted by the model based on the analytical solutions to the equations of heat transfer and species diffusion inside droplets, are compared for the values of parameters relevant to experimental set-up described in Section 4.3 and other related conditions. The effect of the choice of the binary diffusion coefficient correlation on droplet heating and evaporation for experimental conditions described in Section 4.3 is discussed in Section 4.7. The main results of this chapter are summarised in Section 4.8.

4.2 Basic equations and approximations

The model developed in this chapter is based on the equations describing liquid phase heating and evaporation, species diffusion in the liquid phase and species mass fractions at the surface of the droplets. These equations and their approximations and analytical solutions, where appropriate, are presented and discussed below.

4.2.1 Droplet heating

The process of heating (or cooling) for stationary spherically-symmetric multi-component droplets is the same as in the case of mono-component droplets (Sazhin et al, 2004), described in Chapters 2 and 3, where the temperature of the droplet õ G,E can be calculated from Eq. (2.23). This model is equally applicable to mono-component and multi-component droplets. The physical properties of multi-component droplets are calculat

$$\grave{A}_Z \quad \frac{*}{\backslash u_{\hat{A}} \backslash^{2}} \acute{I}_Y^{*} \quad {}_Y \; \text{ç} \;\;]_Z \;\; \text{ç} \;\; \mathbf{d}\text{ç}, \tag{4.20}$$

$$\text{ç} \quad \frac{7}{7_8 \;\; ?}, \;]_Z \;\; \text{ç} \qquad \mathbf{sin} \;\; \text{ç}X_Z \;\; ,$$

$$_Y \;\; \text{ç} \qquad E_{DY}^{\;/+} \text{ç} \;\; {}_Y \;\; \text{ç}E_{DY} \;\; \mathbf{exp} \; \frac{7_8^{@} \;\; ? \;\; 7_{8Æ}}{A} \text{ç}^{+} \;\; . \tag{4.21}$$

We should notice the difference between the parameters $_Y$, $\backslash\,]_Z \backslash^{+}$ and $\grave{A}_Z$

A countable set of positive solutions to this equation (positive eigenvalues) are arranged in ascending order, as in the case of Solutions (2.23), (D.38) and (4.15).

4.2.6 Numerical solutions

We will use two solutions to heat transfer and species diffusion equations; the one based on the analytical solutions to Eqs. (2.21) and (4.4) and the other based on the numerical solutions to these equations. These are referred to as Solutions A and B respectively.

The Cranck-Nicholson method is used to solve numerically Eqs. (2.21) and (4.4). This classical approach has already been used in several papers, including Abramzon and Sirgnano (1989) and Maqua et al (2008), to describe the droplet heating and the change of its composition.

In this chapter, the results of the numerical solutions are provided by Dr. Guillaume Castanet. The timestep is set at 0.01 ms and the radius of the droplet is divided into 200 elements of identical size, which appears to be sufficient to ensure a good accuracy in the results. The dependence of liquid properties on temperature and composition is taken into account while the gas properties are assumed to be the same as air and they depend on temperature. A54( )-80.1938(0)-0.295 5436(u)-0.2955585

As follows from Figs. 4.2 and 4.3, all three temperatures are well separated for both acetone and ethanol. Hence, the difference between them needs to be taken into account in the analysis of experimental data. In the case of acetone there seems to be a reasonable agreement between the values of average temperature of the droplets and experimental data. Data on the time evolution of droplet radii were not available. Note that the Effective Thermal Conductivity and Effective Diffusivity models, on which the analysis of this chapter is based, are primarily designed to predict correctly the average surface temperature and species mass fractions of droplets, but not their average temperature and species mass fractions.

In the case of pure ethanol shown in Fig. 4.3, the

In Fig. 4.4 (25% ethanol - 75% acetone; the case of acetone dominated mixture), the agreement between the observed and predicted average droplet temperatures, for both ideal and non-ideal models, is reasonably good, although the scatter of experimental data in this case is more noticeable than in the case of pure acetone shown in Fig. 4.2.

In Fig. 4.5 (the case of the 50% ethanol - 50% acetone mixture), the experimentally observed temperatures lie between the average and surface temperatures predicted by both ideal and non-ideal models. These temperatures are closer to the average temperatures predicted by the non-ideal model than to those predicted by the ideal model.

Fig. 4.6 The same as Figs. 4.4 and 4.5 but for the 75% ethanol–25% acetone mixture

Fig. 4.8 The plots of

Fig. 4.9 The plots of versus $/ _d$ for six moments of time after the start of calculations for the same droplets as in Figs. 4.6-4.8.

Fig. 4.10 The plots of the ethanol mass fraction Y_l versus $/ _d$

Fig. 4.14 The same as Fig. 4.13 but for pure ethanol droplets.

In the case of acetone (see Fig. 4.13), the observed temperature values lie close to the average temperatures. In the case of ethanol (see Fig. 4.14), the observed temperatures are close to or below the surface temperature of the droplets. Hence, for both acetone and ethanol, the trends of predicted temperatures agree with experimental observations, but there is a rather poor agreement between the values of observed and predicted temperatures for both acetone and ethanol, in agreement with results shown in Figs. 4.2 and 4.3, as the measured temperatures are expected to be the volume-averaged droplet temperatures with systematically more weighting in the zones near the centres of the droplet (see Section 4.3). The reason for this lack of quantitative agreement is not clear to us.

However, both these models predict about the same trend in the evolution of temperature with time. The ideal model can be used if the prediction errors of several degrees can be tolerated. This seems to be our case where the random errors of the estimates of droplet temperatures appear to be about 2-3 degrees. As in the cases shown in Figs. 4.13 and 4.14, the results predicted by Solutions A and B coincide within the accuracy of plotting, which gives us confidence in the results predicted by both solutions.

In the case of an acetone dominated mixture (25% ethanol – 75% acetone: see Fig. 4.15), the agreement between the observed and predicted average droplet temperatures, for both ideal and non-ideal models, is reasonably good. Most of the observed temperatures lie between average and centre temperatures, although the scatter of experimental data in this case is more noticeable than for pure acetone (see Fig. 4.13).

In the case of the 50% ethanol – 50% acetone mixture (see Fig. 4.16), the experimentally observed temperatures lie closer to average temperatures predicted by the non-ideal model. For the 75% ethanol – 25% acetone mixture (see Fig. 4.17),

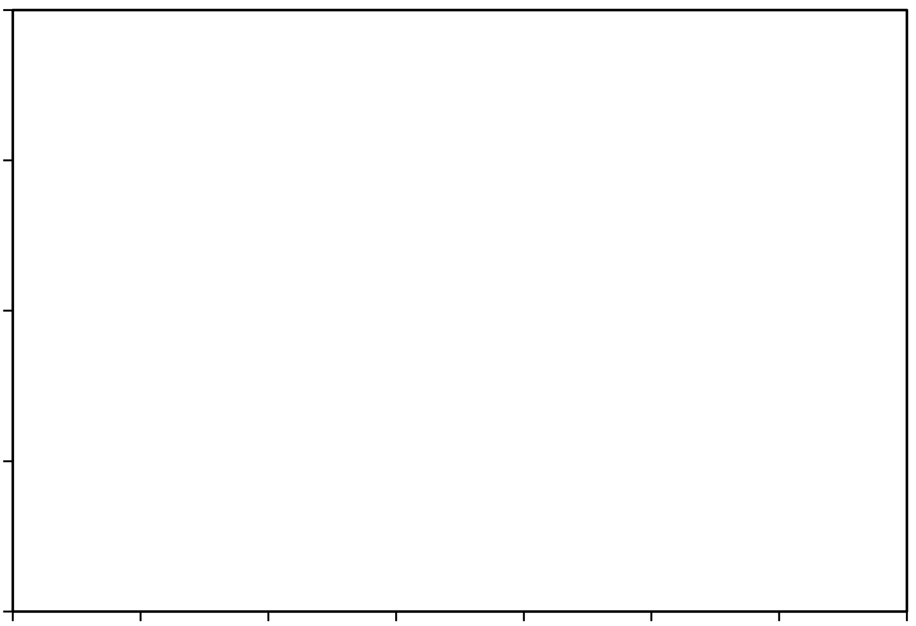

Fig. 4.17 The same as Figs. 4.15 and 4.16 but for the 75% ethanol – 25% acetone mixture droplets.

4.4.3 Solution A based on moving boundary

As mentioned in the Introduction, in a number of pa